Multiscale Science and Engineering (2023) 5:133–146
https://doi.org/10.1007/s42493-024-00100-2

REVIEW

Advancements and Challenges of Micromechanics-based Homogenization for the Short Fiber Reinforced Composites

Hugon Lee[1] · **Sangryun Lee**[2] · **Seunghwa Ryu**[1]

Received: 1 November 2023 / Revised: 6 December 2023 / Accepted: 7 December 2023 / Published online: 6 March 2024

Abstract

In the realm of technologically important short fiber and particulate-reinforced composites, homogenization approaches based on micromechanics are extensively explored for estimating inherent effective properties. This review provides a comprehensive overview of the core principles underpinning micromechanics-based homogenization, as well as its advancements and applications encompassing: (i) predicting nonlinear reactions under complex and cyclic loading conditions, (ii) accounting for interfacial imperfections, and (iii) estimating various effective physical properties. We also delve into the integration of (iv) data-driven strategies, aiming to augment the accuracy of predictions. We conclude the article by discussing a seminal challenge, (v) the prediction of localized failure.

Keywords Homogenization · Micromechanics · Nonlinear · Interfacial Imperfection · Data-driven

Introduction

Composite materials, composed of two or more distinguishable phases, offer distinct advantages by synergistically enhancing material properties across a wide array of applications. Their phases are typically referred as primary phase (called matrix) and secondary phases (called inclusion, inhomogeneity, filler, or reinforcement). In order to achieve efficient utilization of composites, understanding the properties of the material, which heavily relies on factors including shape, volume fraction, and spatial arrangement of the reinforcements, is crucial. In situations where the reinforcements maintain regular and periodic structures, an analytical model considering load transfer in a single unit cell (or, representative volume element) can be a good representation. This is evident in synthetic composites with continuous fiber reinforcements [1] and nature-inspired staggered platelet structures [2, 3]. On the other hand, composites with short-fiber fillers or spherical reinforcements utilized random arrangements, making it infeasible to handle intricate interaction and load transfer characteristics. In such cases, micromechanics-based homogenization emerges as a valuable tool, providing predictions with acceptable accuracy while significantly reducing computational costs compared to numerical analysis employing fine microstructures.

Early investigations on effective mechanical properties of short-fiber reinforced composites and multicomponent alloys are based on computing the strain fields in each phase [4]. Notably, when the volume fraction of reinforcements in a composite is low (less than 20%), accounting for their influence can effectively addressed via a mean-field strategy. The method assumes the surrounding area of reinforcements as if it's part of the matrix affected by a strain similar to the matrix's overall average strain (Mori-Tanaka method) [5] or alternatively, by using a medium mirroring the composite's effective stiffness (self-consistent method) [6]. Upon the mean-field approximation, the composite's effective properties, considering multiple reinforcements, can be determined by utilizing solutions of single inhomogeneity problems.

Following the establishment of the homogenization scheme for linear elastic responses, its application expanded to encompass various aspects of composite characteristics.

✉ Sangryun Lee
sr.lee@ewha.ac.kr

✉ Seunghwa Ryu
ryush@kaist.ac.kr

[1] Department of Mechanical Engineering, Korea Advanced Institute of Science and Technology, Daejeon 34141, Republic of Korea

[2] Division of Mechanical and Biomedical Engineering, Ewha Womans University, Seoul 03760, Republic of Korea

To model the nonlinear inelastic behaviors of composites, linear approximation techniques detailed in several studies were employed [7–15]. Furthermore, the emergence of nanocomposites featuring nanoscale reinforcements has prompted considerable interest in modeling the effects of imperfect matrix-reinforcement interfaces, primarily due to their substantial interface-to-volume ratio. Owing to the mathematical similarity between the governing equations of diverse phenomena and elasticity, the mathematical framework has been instrumental in predicting a wide range of effective physical properties. Additionally, the advent of diverse machine learning techniques has emphasized data-driven methodologies as potential solutions to reconcile disparities between predictions from homogenization theory and experimental outcomes. This is particularly crucial when dealing with high volume fractions of reinforcement, inadequately modeled interfacial imperfections, and when uncertainties within microstructure persist.

In this review, we present the advancements and applications pertinent to aforementioned aspects of homogenization theory. Section "Mathematical Foundation of Micromechanics-Based Homogenization Theory" briefly introduces the mathematical foundation of micromechanics-based homogenization theory. Extensions to nonlinear mechanical responses are addressed in Sect. "Extension to Nonlinear Mechanical Response". Section "Effect of Interfacial Imperfection" delves into the considerations of the effect of interfacial imperfection. In Sect. "Extension to Various Physical Properties", we explore the extensions of the homogenization theory to predict various other physical phenomena. Section "Combining Data-Driven Methods" addressed the data-driven approach utilizing multi-fidelity dataset (homogenization theory prediction with experimental or direct numerical simulation data) to enhance prediction accuracy. Conclusions and future direction are outlined in Sect. "Conclusion", with a particular focus on predicting the localized failures in composites.

Throughout this paper, unless specified otherwise, the following conventions for mathematical expressions are utilized. Boldface letters indicate vectors or tensors, while non-boldface letters indicate scalar values. Both tensorial and indicial notations following Einstein's summation convention are used. Subscripts 0 and 1 assigned to tensors and scalars denote the matrix and reinforcement phases, respectively. The operation $(:)$ denotes a double contraction and is computed as follows, for second-order tensors $\boldsymbol{a}$ and $\boldsymbol{b}$, and fourth-order tensors $\boldsymbol{A}$ and $\boldsymbol{B}$:

$$\boldsymbol{a} : \boldsymbol{b} = a_{ij}b_{ij}, \quad (\boldsymbol{A} : \boldsymbol{b})_{ij} = A_{ijkl}b_{kl}, \quad (\boldsymbol{A} : \boldsymbol{B})_{ijkl} = A_{ijmn}B_{mnkl}.$$

Mathematical Foundation of Micromechanics-Based Homogenization Theory

In this section, the basic mathematical foundation of the micromechanics is introduced within the context of linearized elasticity under small deformation. In Fig. 1a-b, the stress distribution within matrix and reinforcements during uniaxial tensile loading of particulate composites is illustrated while the reinforcement volume fraction is denoted as c_1. In the case of a high reinforcement volume fraction (Fig. 1a), the stress distribution, and thus strain distribution, within reinforcements is non-uniform, while in the case of a low volume fraction (Fig. 1b), the stress and strain field within reinforcements appears uniform. It is worth noting that while we have visualized spherical reinforcements, the same observations can apply to ellipsoidal ones. It can be inferred that when the distance between reinforcements is relatively large and the shape of the reinforcement is ellipsoidal, the strain field within the reinforcements tends to become uniform.

In the case of a single inhomogeneity as depicted in Fig. 1c, it is mathematically established that the strain field within an ellipsoidal inhomogeneity becomes uniform. Consequently, when the volume fraction of reinforcement is relatively low, usually less than 20%, it becomes feasible to approximate the average strain field within the reinforcements by embedding a single inhomogeneity within a matrix under the influence of the average strain field of the multi-component composites, a method commonly referred to as the mean-field approximation. In the Mori-Tanaka mean-field homogenization scheme, the relation between the average strain fields in the matrix, inhomogeneity, and composite (represented as $\overline{\boldsymbol{\varepsilon}}_0, \overline{\boldsymbol{\varepsilon}}_1$, and $\overline{\boldsymbol{\varepsilon}}(= \boldsymbol{\varepsilon}^A$, applied strain), respectively) are related as follows [5]:

$$\overline{\boldsymbol{\varepsilon}}_1 = \boldsymbol{T} : \overline{\boldsymbol{\varepsilon}}_0 = \boldsymbol{T} : \left(c_0\boldsymbol{I} + c_1\boldsymbol{T}\right)^{-1} : \overline{\boldsymbol{\varepsilon}} = \boldsymbol{A} : \overline{\boldsymbol{\varepsilon}}, \tag{1}$$

where $\boldsymbol{A} = \boldsymbol{T} : \left(c_0\boldsymbol{I} + c_1\boldsymbol{T}\right)^{-1}$ is the strain concentration tensor in Mori-Tanaka method, and $I_{ijkl} = \frac{1}{2}\left(\delta_{ik}\delta_{jl} + \delta_{il}\delta_{jk}\right)$ represents the fourth-order symmetric identity tensor with δ_{ij} denoting Kronecker delta symbol. As the volume fraction c_1 of inhomogeneity tends towards very small values (i.e., the matrix volume fraction becomes very large, $c_0 \approx 1$), the tensor $\boldsymbol{A}$ converges to $\boldsymbol{T}$, which is the strain concentration tensor for single inhomogeneity problem. By considering the volume-averaged stress and strain fields within both the matrix and reinforcement ($\overline{\boldsymbol{\sigma}} = c_0\overline{\boldsymbol{\sigma}}_0 + c_1\overline{\boldsymbol{\sigma}}_1 = c_0\boldsymbol{L}_0 : \overline{\boldsymbol{\varepsilon}}_0 + c_1\boldsymbol{L}_1 : \overline{\boldsymbol{\varepsilon}}_1$ and $\overline{\boldsymbol{\varepsilon}} = c_0\overline{\boldsymbol{\varepsilon}}_0 + c_1\overline{\boldsymbol{\varepsilon}}_1$, respectively), it becomes possible to predict the effective stiffness ($\boldsymbol{L}_{\text{eff}}$) in the Mori-Tanaka scheme for composites as follows [5]:

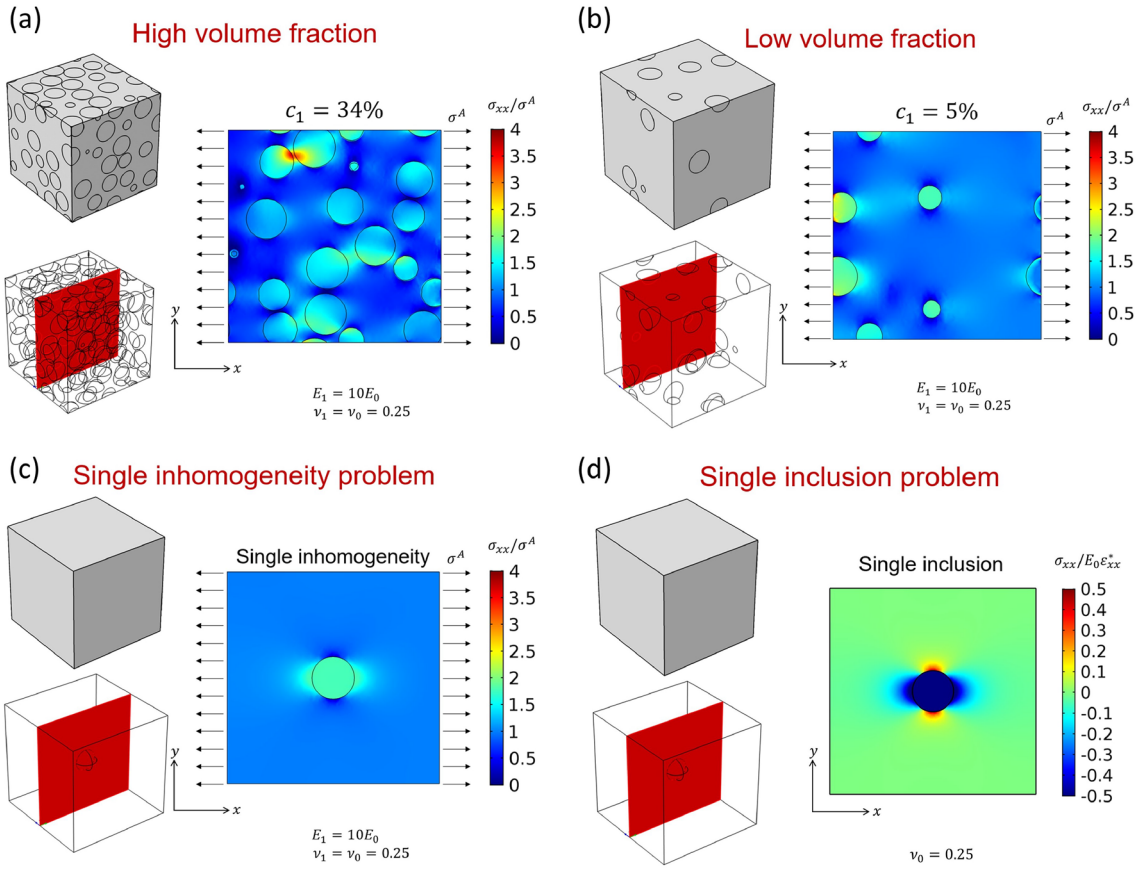

Fig. 1 Stress field within **a** composites including high volume fraction inhomogeneities, **b** low volume fraction inhomogeneities, **c** single inhomogeneity, and **d** single inclusion. The visualizations are within a cross-section of a three-dimensional volume. The inhomogeneity Young's modulus, E_1, is set to be 10 times larger than the matrix modulus, E_0, where Poisson's ratio, ν, for both phases are set to be equal. The tensile stress in x-direction, σ_{xx}, is visualized which is normalized by applied stress, σ^A, for (**a**–**c**) and eigenstress, $\sigma^*_{xx} = E_0\varepsilon^*_{xx}$, for (**d**)

$$\overline{\boldsymbol{\sigma}} = \boldsymbol{L}_{\text{eff}} : \overline{\boldsymbol{\varepsilon}} \text{ where } \boldsymbol{L}_{\text{eff}} = \left(c_0\boldsymbol{L}_0 + c_1\boldsymbol{L}_1 : \boldsymbol{T}\right) : \left(c_0\boldsymbol{I} + c_1\boldsymbol{T}\right)^{-1}, \tag{2}$$

where $\boldsymbol{L}_0$ and $\boldsymbol{L}_1$ refer to the stiffness tensors of matrix and reinforcement, respectively.

However, obtaining the strain field distribution for the single inhomogeneity problem remains a challenging mathematical task. To apply Green's function-based solutions typically used for homogeneous media, it is necessary to identify an equivalent single inclusion (in micromechanics, an inclusion refers to a material with an elastic stiffness tensor identical to that of the matrix). Thanks to Eshelby's contributions [16, 17], in the case of a single inhomogeneity problem where the applied strain is $\boldsymbol{\varepsilon}^A$, one can establish an equivalent inclusion problem by introducing the concept of an inclusion with an eigenstrain $\boldsymbol{\varepsilon}^{*,\text{Eq}}$, referred as equivalent eigenstrain, embedded within the matrix since the strain inside ellipsoidal inclusion is uniform for the single inclusion problem (Fig. 1d). The eigenstrain of the equivalent problem can be expressed as follows [4]:

$$\left[\left(\boldsymbol{L}_1 - \boldsymbol{L}_0\right) : \boldsymbol{S} + \boldsymbol{L}_0\right] : \boldsymbol{\varepsilon}^{*,\text{Eq}} = \left(\boldsymbol{L}_1 - \boldsymbol{L}_0\right) : \boldsymbol{\varepsilon}^A. \tag{3}$$

Here, $\boldsymbol{S}$ refers to the fourth-order Eshelby tensor, which establishes a connection between the eigenstrain $\boldsymbol{\varepsilon}^*$ of free-standing inclusion and the constrained strain $\boldsymbol{\varepsilon}^c$ embedded in a matrix through [4]:

$$\boldsymbol{\varepsilon}^c = \boldsymbol{S}{:}\boldsymbol{\varepsilon}^* \text{ where } S_{ijrs} = \frac{1}{2}\int_{\Omega} L^0_{pqrs}\left\{\frac{\partial^2 G_{ip}(\boldsymbol{x}-\boldsymbol{y})}{\partial x_j \partial y_q} + \frac{\partial^2 G_{jp}(\boldsymbol{x}-\boldsymbol{y})}{\partial x_i \partial y_q}\right\} d\boldsymbol{y}, \tag{4}$$

where Ω refers to the domain of inclusion and $G_{ip}(\boldsymbol{x}-\boldsymbol{y})$ is Green's function indicating the i-th component of displacement field at location $\boldsymbol{x}$, when point unit force along p-th direction applied at the location $\boldsymbol{y}$. L^0_{pqrs} represents the indicial notation of matrix elastic stiffness tensor $\boldsymbol{L}_0$. Based on the equivalent problem, the concentration tensor $\boldsymbol{T}$ for single inhomogeneity problem can be expressed in terms of Eshelby tensor as $\boldsymbol{T} = \left[\boldsymbol{I} + \boldsymbol{S} : \boldsymbol{L}_0^{-1} : \left(\boldsymbol{L}_1 - \boldsymbol{L}_0\right)\right]^{-1}$. In

other words, combining Equations (1) and (2), the effective modulus can be obtained easily if the expression for the Eshelby tensor is given. The Eshelby tensor depends on the shape of the inclusion and does not change over the size because there is no characteristic length scale in elasticity. In contrast, in the presence of an interfacial imperfection, the modified Eshelby tensor depends on the absolute size of the inclusion, which will be discussed in Sect. "Effect of Interfacial Imperfection".

One has to note that the aforementioned equations are valid if all short fiber reinforcements are ellipsoidal and aligned perfectly along one direction. In cases involving more realistic reinforcements like cylindrical fibers or carbon nanotubes, their shapes are approximated as prolate ellipsoids, and the corresponding Eshelby tensor expression is applied. Similarly, for graphene and other plate-type reinforcements, their shapes are approximated as oblate ellipsoids. To account for the orientation distribution of reinforcements, one can use orientation averaged Mori-Tanaka method as [18]:

$$\boldsymbol{L}_{\text{eff}} = \left(c_0\boldsymbol{L}_0 + c_1\langle \boldsymbol{L}_1 : \boldsymbol{T}\rangle\right) : \left(c_0\boldsymbol{I} + c_1\langle \boldsymbol{T}\rangle\right)^{-1}, \tag{5}$$

where the operator $\langle\cdot\rangle$ denotes the orientation average of each tensor.

Throughout this section, we employed the term inclusion for materials possessing identical material properties to the matrix and inhomogeneity for materials that can have different material properties compared to the matrix during the development of homogenization theory. However, in numerous contexts not related to the theory's development via the equivalent inclusion approach, these terms are used interchangeably. Hence, the subsequent sections will use the term inclusion for general secondary phases in composites, which may have either the same or different properties compared to the primary phase, i.e., the matrix.

Extension to Nonlinear Mechanical Response

After investigations into mean-field homogenization methods applicable to linear systems, specifically linear elasticity with infinitesimal deformation kinematics, researchers have made significant efforts to extend this theory to encompass more general nonlinear mechanical responses. These responses include nonlinear constitutive relations (material nonlinearity) and finite deformation kinematics (geometric nonlinearity). In the early stage of exploration, several studies attempted to apply homogenization techniques in the Laplace-Carson domain by employing the correspondence principles to account for viscoelastic and elastic-viscoplastic behavior [19–26]. However, these approaches encountered significant mathematical complexity when dealing with inverse transforms.

As a result, recent studies have adopted a time-domain homogenization approach, where a virtual heterogeneous linear material with similar underlying microstructure is introduced to estimate the effective behavior of the original nonlinear material [27]. This virtual linear material is known as the linear comparison composite (LCC) [11]. In this approach, a suitable linear homogenization method, such as the Mori-Tanaka method, is applied to the formulated LCC to express its effective behavior. The formulation of LCC can be achieved through two main approaches: variational formulations [15, 28] and the linearization of local constitutive models [9, 29, 30]. The choice between using tangent or secant operators depends on the specific linearization scheme employed. Despite the substantial body of literature dedicated to nonlinear mean-field homogenization theory, there remains an ongoing debate regarding which framework offers the most numerically efficient and mathematically rigorous predictions.

Among the various models, an incremental affine formulation, developed by drawing analogies between thermoelasticity and linearized elasto-viscoplasticiy [31] or viscoelasticity-viscoplasticity [32], possesses a significant advantage. This formulation is applicable to multiaxial loading cases with arbitrary loading histories, without relying on empirical parameters. However, this method does have a drawback in that it tends to produce overly stiff predictions in the viscoelastic regime, which becomes even more pronounced in the context of finite deformations. To address this issue, heuristic isotropitization techniques [33, 34] or regularization methods [31, 32] have been applied to soften the predictions. It is important to note that these techniques lack substantial mathematical or physical justification [35].

To address this issue without resorting to the aforementioned techniques, an adaptive affine scheme [36, 37] has introduced a method to dynamically correct the inconsistency in the stress state for each time step during the homogenization process. The original issue of inconsistency in the incremental affine formulation stems from the changing modulus over time increments, leading to a discrepancy in the average strains across different phases due to alterations in the strain concentration tensors. This inconsistency accumulates as a result of repeated incremental deformation procedures. The adaptive scheme [36] incorporates a fictitious uniform strain ($\Delta\boldsymbol{\epsilon}^*$, distinct from the eigenstrain discussed in Sect. "Mathematical Foundation of Micromechanics-Based Homogenization Theory") into each phase to ensure the consistency of the strain, where

the strains are related by the equation $\boldsymbol{\varepsilon}_1 = \boldsymbol{B}_1^{\varepsilon} : \boldsymbol{\varepsilon}_0$. Here, $\boldsymbol{B}_1^{\varepsilon} = \left[\boldsymbol{I} + \boldsymbol{S} : \boldsymbol{L}_0^{-1} : \left(\boldsymbol{L}_1 - \boldsymbol{L}_0\right)\right]^{-1}$ is the strain concentration tensor of the Mori-Tanaka scheme, corresponding to the $\boldsymbol{T}$ tensor discussed in the previous section. Upon the incorporation of the fictitious strain, the stress state within each phase is modifies as follows [36]:

$$\boldsymbol{\sigma}_i^* = \boldsymbol{L}_i : \Delta\boldsymbol{\varepsilon}^* + \boldsymbol{\sigma}_i\left(t_n\right), \tag{6}$$

where subscript i takes the values of 0 for matrix, and 1 for inclusion. By tuning the fictitious strain to ensure consistency at t_{n+1} with relation

$$\boldsymbol{L}_1^{-1}\left(t_{n+1}\right) : \boldsymbol{\sigma}_1^* = \boldsymbol{B}_1^{\varepsilon} : \boldsymbol{L}_0^{-1}\left(t_{n+1}\right) : \boldsymbol{\sigma}_0^*, \tag{7}$$

the strain is expressed as follows:

$$\Delta\boldsymbol{\varepsilon}^* = \left(\boldsymbol{I} - \boldsymbol{B}_1^{\varepsilon}\right)^{-1} : \left[\boldsymbol{B}_1^{\varepsilon} : \boldsymbol{L}_0^{-1}\left(t_{n+1}\right) : \boldsymbol{\sigma}_0\left(t_n\right) - \boldsymbol{L}_1^{-1}\left(t_{n+1}\right) : \boldsymbol{\sigma}_1\left(t_n\right)\right]. \tag{8}$$

Subsequently, following the same principles as the original incrementally affine method, an identical macro strain is applied to the composite to eliminate the fictitious deformation. The process is illustrated in Fig. 2a, and the incremental strain change, which represents the adaptive strain correction for the n-th time step $[t_n, t_{n+1}]$, of the inclusion at the consistency state is given by [36]:

$$\begin{aligned}\Delta\boldsymbol{\varepsilon}_1^{*,n} = c_0\boldsymbol{A}_1^{\varepsilon}:&\left(\boldsymbol{L}_0^{-1}:\boldsymbol{\sigma}_0\left(t_n\right) - \left[\boldsymbol{I} + \boldsymbol{S}:\boldsymbol{L}_0^{-1}:\left(\boldsymbol{L}_1 - \boldsymbol{L}_0\right)\right]:\right.\\ &\left.\boldsymbol{L}_1^{-1}:\boldsymbol{\sigma}_1\left(t_n\right)\right),\end{aligned} \tag{9}$$

where $\boldsymbol{A}_1^{\varepsilon} = \boldsymbol{B}_1^{\varepsilon} : \left[c_0\boldsymbol{I} + c_1\boldsymbol{B}_1^{\varepsilon}\right]^{-1}$ in Mori-Tanaka scheme. Meanwhile, the incremental strain change for the matrix can be calculated via $\Delta\boldsymbol{\varepsilon}_0^{*,n} = -\left(c_1/c_0\right)\Delta\boldsymbol{\varepsilon}_1^{*,n}$.

The prediction of the framework compared to direct numerical simulation of representative volume elements is illustrated in Fig. 2b-c, showcasing its effectiveness in both monotonic and cyclic loading scenarios. Through adaptive adjustment to address the common inconsistency issue prevalent in existing homogenization theories, a good agreement with the results of finite element method (FEM) simulation is achieved. This correction is particularly crucial in cases involving significant change in modulus.

The fundamental concept of adaptive correction is believed to be applicable to various homogenization models that are based on LCC schemes. It is important to note that this validation is conducted for relatively small inclusion volume fraction of 15%, where the validity of linear homogenization schemes like the Mori-Tanaka method is assured. To achieve high accuracy over a broader range of volume fractions, further investigation into improved linear homogenization methods, suitable linearization schemes, and their combined effect is expected to be of paramount

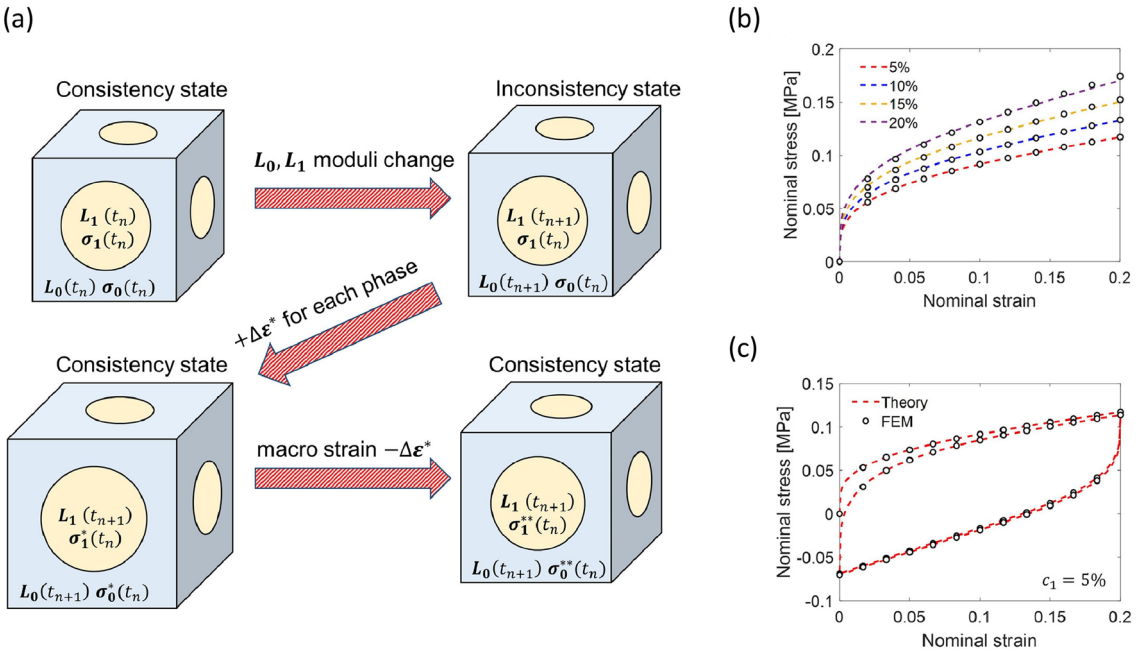

Fig. 2 **a** Schematics of adaptive affine homogenization scheme for nonlinear constitutive laws by adaptively correcting strain increments with fictitious uniform strain $\Delta\boldsymbol{\varepsilon}^*$ to satisfy consistent stress concentration between phases. Nonlinear homogenization prediction of stress-strain curves compared to FEM simulations for monotonic (**b**) and cyclic (**c**) loading cases. The legends in (**b**) as well as c_1 in (**c**) designate inclusion volume fraction, while white dots designate FEM data for both (**b**) and (**c**). Reproduction with permission from Ref. [36] Copyright (2022) Elsevier

importance [38]. One potential approach to enhance accuracy could involve the adoption of second-order homogenization techniques that take into account second-order statistical moments of the fields [27, 33, 39].

Effect of Interfacial Imperfection

In real composite materials, produced through diverse manufacturing processes, imperfections at the interfaces between phases are inevitable. These imperfections stem from factors such as manufacturing-induced defects or inherent lattice mismatches. Consequently, interfacial imperfections can lead to phenomena like debonding or slippage, resulting in displacement jumps in elasticity. Researchers such as Qu, J. [40] and Lee, S. et al. [41, 42], among others, have extensively studied and described these phenomena. Various method exist to characterize interfacial imperfections in elasticity [43, 44]. However, in this review, we primarily concentrate on the interface spring model [40], owing to its mathematical simplicity. Towards the end of this section, we briefly touch upon the interphase model [45], recognizing its usefulness for certain cases.

Within the framework of the interface spring model, a virtual spring layer characterized by an infinitesimal thickness is positioned between the matrix and inclusion, as illustrated in Fig. 3a, utilizing displacement jump. The compliance of the spring ($\boldsymbol{\eta}$), which is a second-order tensor, can be written in terms of compliances in the normal direction (α) and tangential direction (β) as follows [40]:

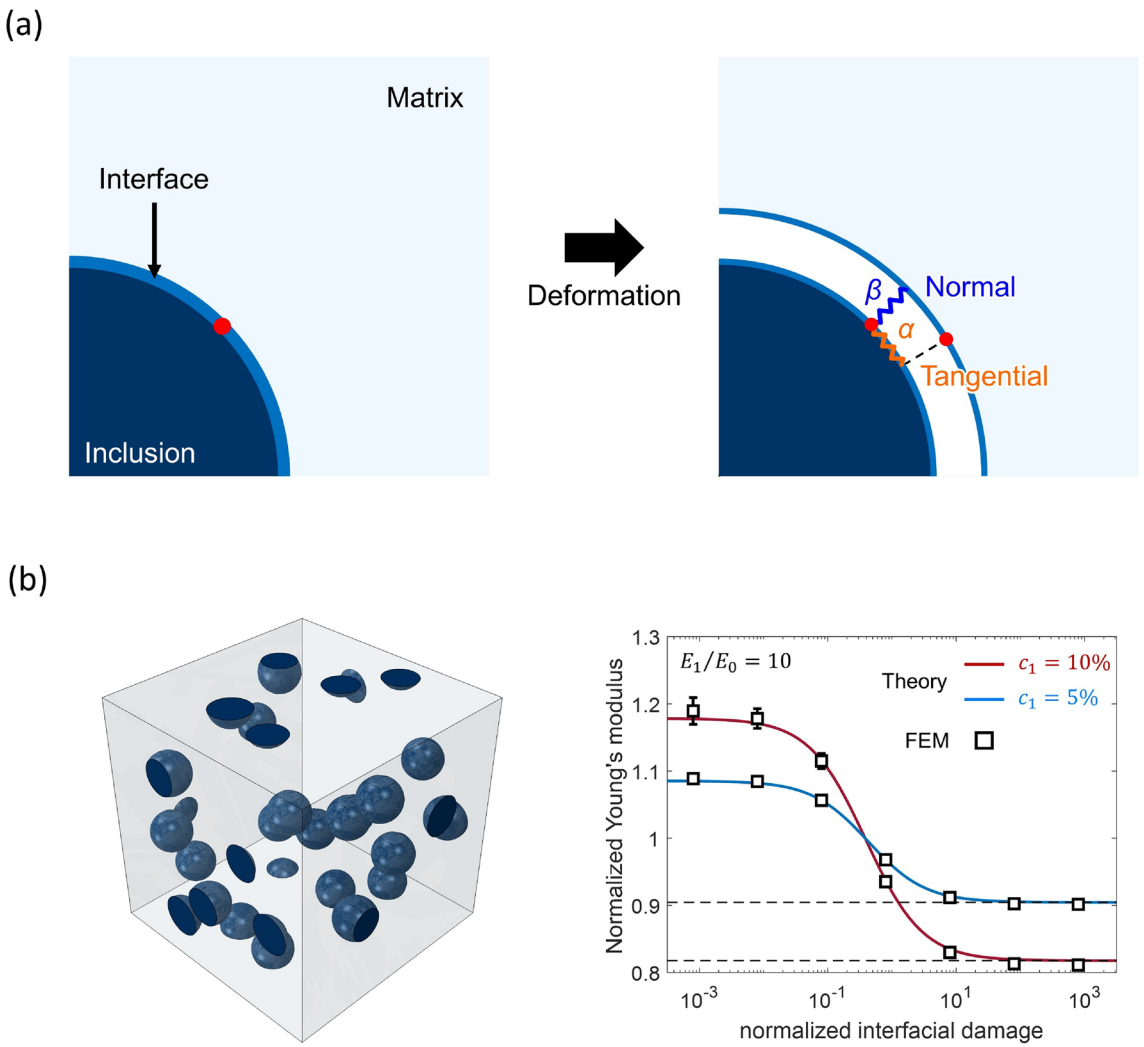

Fig. 3 **a** Schematics of interface spring model with springs in normal and tangential directions. **b** Representative volume element of randomly generated spherical inclusions with 0.05 volume fraction, and estimation of effective Young's modulus by homogenization theory compared to FEM results. The FEM results are averaged over 10 realizations allowing the overlap between phases. This figure is adopted from Ref. [42] with permission Copyright (2019) Sage Publications, and also from Ref. [46] under Creative Commons Attribution License (CC BY)

$$\eta_{ij} = \alpha\delta_{ij} + (\beta - \alpha)n_i n_j, \tag{10}$$

where $\boldsymbol{n}$ is the unit outward normal vector of the inclusion surface. When the inclusion takes the form of a perfect sphere, and the normal and tangential compliances are identical, denoted as $\alpha = \beta \equiv \gamma_s$, the inclusion exhibits uniform strain field [47]. Consequently, for such cases, a closed-form expression of modified Eshelby tensor can be derived. In our previous study, we demonstrated and numerically validated the expression for the modified Eshelby tensor, given by [41]:

$$\boldsymbol{S}^M = \left[\boldsymbol{I} + \frac{\gamma_s}{R}(\boldsymbol{I} - \boldsymbol{S}) : \boldsymbol{L}_0\right]^{-1} : \left[\boldsymbol{S} + \frac{\gamma_s}{R}(\boldsymbol{I} - \boldsymbol{S}) : \boldsymbol{L}_0\right], \tag{11}$$

where R is the radius of the spherical inclusion. The modified strain concentration tensor within the Mori-Tanaka scheme is written as:

$$\boldsymbol{T}^M = \left(\boldsymbol{I} + \boldsymbol{S} : \boldsymbol{L}_0^{-1} : (\boldsymbol{L}_1 - \boldsymbol{L}_0) + \frac{\gamma_s}{R}(\boldsymbol{I} - \boldsymbol{S}) : \boldsymbol{L}_1\right)^{-1}. \tag{12}$$

The composite effective modulus is derived as [42]:

$$\boldsymbol{L}_{\text{eff}} = \left(c_0\boldsymbol{L}_0 + c_1\boldsymbol{L}_1 : \boldsymbol{T}^M\right) : \left(c_0\boldsymbol{I} + c_1\boldsymbol{T}^M + c_1\frac{\gamma_s}{R}\boldsymbol{L}_1 : \boldsymbol{T}^M\right)^{-1}. \tag{13}$$

The validation of the effective modulus prediction using Equation (13) is conducted through comparison with finite element method (FEM) analysis of a representative volume element. Fig. 3b illustrates the effective Young's modulus normalized by matrix modulus (E_{eff}/E_0) plotted against the normalized interfacial damage parameter ($\mu_0\gamma_s/R$), where μ_0 represents the shear modulus of the matrix. The visualization in the figure also showcases randomly positioned spherical inclusions with a volume fraction of $c_1 = 0.05$. In the limiting case of very small interfacial damage (i.e., very small compliance), the effective modulus approaches the prediction considering no interfacial damage. As the interfacial compliance increases (signifying a gradual reduction in load transfer through reinforcements), the effective modulus tends towards the value of a porous medium, with a void volume fraction equivalent to that of the inclusion. Here, one can notice that the higher volume fraction of stiffer reinforcements may decrease the effective modulus of composites if the interfacial imperfection is large. Detailed discussion on the effect of volume fraction, reinforcement size, comparison with FEM calculations can be found from our earlier studies on these subjects [41, 42].

It's noteworthy that the model is particularly suitable for spherical inclusions. Even slight deviations from a spherical inclusion shape can introduce significant non-uniform interior fields [40–42, 48]. Additionally, to leverage the uniform interior fields, it becomes crucial to match the normal and tangential spring compliances. These constraints limit the applicability of the homogenization theory derived considering the uniform interior strain field. Therefore, prior to applying the interface spring model, it's imperative to thoroughly verify the model's validity concerning the shape of inclusions and the compliances of springs. Moreover, the correct application of modified expressions for $\boldsymbol{S}^M$ (Equation 11), $\boldsymbol{T}^M$ (Equation 12), and $\boldsymbol{L}_{\text{eff}}$ (Equation 13), which differ from their perfect interface counterparts, should be carefully examined.

On the other hand, another limitation of the interface spring model is its allowance for unphysical overlapping of phases. Notably, the FEM result presented in Fig. 3b assumes no contact between phases, permitting such overlapping as per the assumptions of the theory. When a uniaxial load is applied to the composite, the material contracts perpendicular to the load direction due to the Poisson effect. This contraction leads to an overlap between the matrix and the inclusion. Introducing the non-overlapping condition in numerical simulations causes analytical predictions deviate from the numerical prediction. The comparison between theoretical predictions and FEM results considering both overlapping and non-overlapping conditions can be found in our previous work [42]. While an increased disparity observed between theoretical predictions and FEM outcomes when incorporating contact conditions in FEM, it's notable that the difference in effective modulus and the orientation-dependence attributes of stress fields was not markedly substantial.

Lastly, the interface spring model lacks the capability to address the interfacial strengthening effect observed in nanocomposites. To address this limitation, we briefly introduce the interphase model, which accommodates both interfacial strengthening and weakening effects. The interphase model, adopted frequently along with the interface spring model, is used to consider the interfacial imperfection in both normal and tangential directions [49, 50]. This model describes the interface by defining the interphase as a new phase with a finite thickness utilizing different mechanical properties from the matrix and reinforcement. Our previous work has studied the applicability of the two different interface models for nanocomposites by using a series of molecular dynamics simulations [49]. The two models are validated for a wide range of interfacial bond energy. The interface spring model is shown to be reasonable for low interfacial bond energy cases, where the effective modulus decreased upon the decrease in reinforcement size. On the other hand, the interphase model is appropriate for sufficiently high bond energy where the interface has a higher atomic density than that of the pure matrix due to the interatomic interaction between atoms at the reinforcement surface and the higher-order nearest-neighbor atoms in the matrix.

Extension to Various Physical Properties

The developed micromechanics-based homogenization scheme finds application in diverse physical phenomena owing to mathematical similarities. Two distinct categories of steady-state equations governing distinct physics are presented: (i) those related to conductivity/dielectric type equations, and (ii) coupled multi-physics equations. Focusing on the first category concerning conductivity/dielectric-related equations (as summarized in Table 1), the steady-state governing equation is expressed as follows [51]:

$$\boldsymbol{j}(\boldsymbol{x}) = \boldsymbol{K}(\boldsymbol{x}) \cdot \boldsymbol{e}(\boldsymbol{x}) \quad \text{where } \nabla \cdot \boldsymbol{j} = 0, \nabla \times \boldsymbol{e} = \boldsymbol{0}, \tag{14}$$

which is satisfied at any point $\boldsymbol{x}$ within a medium, in the absence of internal sources. The vector fields $\boldsymbol{j}(\boldsymbol{x})$ and $\boldsymbol{e}(\boldsymbol{x})$ exhibit divergence-free and curl-free properties, respectively, while $\boldsymbol{K}(\boldsymbol{x})$ represents a second-order tensor field. The mathematical analogy among these equations allows the homogenization method developed for one of these equations to be readily applied to various physical phenomena outlines in Table 1 for predicting effective properties. However, it should be noted that in the dynamic regime, the governing equations for the different physics are distinct from each other.

Shifting our focus to the second category of coupled multi-physics equations, we delve into the realms of piezoelectric and thermoelectric phenomena. Regarding piezoelectricity, the constitutive relation is expressed as follows [57]:

$$\sigma_{ij} = L_{ijmn}\epsilon_{mn} + d_{nij}\left(-E_n\right),$$

$$D_i = d_{imn}\epsilon_{mn} - \epsilon_{in}\left(-E_n\right), \tag{15}$$

where D_i represents the electrical displacement vector, E_n is the electric vector field, and $\epsilon_{mk} = \left(\frac{\partial D_m}{\partial E_k}\right)_{\varepsilon}$ denotes the symmetric second-order dielectric permittivity constants tensor under constant strain. Additionally, $-d_{ijm} = \left(\frac{\partial \sigma_{ij}}{\partial E_m}\right)_{\varepsilon} = -\left(\frac{\partial D_m}{\partial \epsilon_{ij}}\right)_{E}$ signifies the third-order piezoelectric constants tensor under constant stress, where $d_{kij} = d_{kji}$. σ_{ij}, ϵ_{mn}, and L_{ijmn} denotes stress, strain, and stiffness tensors, respectively, as discussed in previous sections. By employing the notation introduced by Barnett and Lothe [58], the electroelastic moduli C_{iJMn} and constitutive equation are derived as:

$$C_{iJMn} = \begin{cases} L_{iJMn}, & J, M = 1, 2, 3 \\ d_{niJ}, & J = 1, 2, 3; M = 4 \\ d_{iMn}, & J = 4; M = 1, 2, 3 \\ -\epsilon_{in}, & J, M = 4 \end{cases}, \tag{16}$$

$$\Sigma_{iJ} = C_{iJMn} Z_{Mn}.$$

While the notation follows conventional notation, the repeated capital index signifies summation from 1 to 4. Employing this notation allows as to represent the strain and electric fields as:

$$Z_{Mn} = \begin{cases} \epsilon_{Mn}, & M = 1, 2, 3 \\ -E_n, & M = 4 \end{cases}, \tag{17}$$

and the stress and electric displacement fields as:

Table 1 Physical process and related physical quantities following the conductivity/dielectric-related equation, Equation (14), valid under steady-state with no internal sources [51, 52]

Problem	$\boldsymbol{j}$	$\boldsymbol{e}$	$\boldsymbol{K}$
Electrical conduction [53]	Electric current, $\boldsymbol{J}^E$	Electric field, $\boldsymbol{E}$	Electrical conductivity, $\boldsymbol{\sigma}_e$
Dielectrics [53]	Electric displacement, $\boldsymbol{D}$	Electric field, $\boldsymbol{E}$	Dielectric permittivity, $\boldsymbol{\epsilon}$
Magnetism [53]	Magnetic induction, $\boldsymbol{b}$	Magnetic field, $\boldsymbol{h}$	Magnetic permittivity, $\boldsymbol{\mu}_m$
Thermal conduction [54]	Heat flux, $\boldsymbol{q}$	Temperature gradient, $-\nabla T$	Thermal conductivity, $\boldsymbol{\kappa}$
Diffusion [55]	Particle current, $\boldsymbol{j}^N$	Concentration gradient, $-\nabla c$	Diffusivity, $\boldsymbol{D}_f$
Flow in porous media [56]	Weighted fluid velocity, $\eta_v \boldsymbol{j}^f$	Pressure gradient, ∇P	Fluid permeability, $\boldsymbol{k}$

*The symbols in the table correspond to the definitions provided alongside each symbol. In the context of the weighted fluid velocity, $\eta_v \boldsymbol{j}^f$, in porous media flow problems, η_v represents the fluid dynamic viscosity, and $\boldsymbol{j}^f$ denotes the locally averaged fluid velocity within a volume that encompasses both the solid and fluid phases. More comprehensive discussion on the governing equations pertaining to each specific physics involved can be found in the references.

$$\Sigma_{iJ} = \begin{cases} \sigma_{iJ}, & J = 1,2,3 \\ D_i, & J = 4 \end{cases}, \tag{18}$$

Similarly, for a thermoelectricity, the constitutive relation is organized as [59]:

$$\begin{bmatrix} \boldsymbol{J}^E \\ \boldsymbol{J}^S \end{bmatrix} = \begin{bmatrix} \boldsymbol{\sigma}_e & \boldsymbol{\alpha}\cdot\boldsymbol{\sigma}_e \\ \boldsymbol{\alpha}\cdot\boldsymbol{\sigma}_e & \boldsymbol{\gamma}/T \end{bmatrix} \begin{bmatrix} \boldsymbol{E} \\ \boldsymbol{e} \end{bmatrix}, \tag{19}$$

where $\boldsymbol{J}^E$ represents electrical current density, $\boldsymbol{J}^S(=\boldsymbol{q}/T)$ signifies the entropy flux, $\boldsymbol{q}$ is the heat flux, T is the temperature, $\boldsymbol{\sigma}_e$ is the electrical conductivity, $\boldsymbol{\alpha}$ is the Seeback coefficient, $\boldsymbol{\gamma}(=\boldsymbol{\kappa}+T\boldsymbol{\alpha}\cdot\boldsymbol{\sigma}_e\cdot\boldsymbol{\alpha})$ is the thermal conductivity with zero electric field where $\boldsymbol{\kappa}$ is the thermal conductivity at zero current, $\boldsymbol{E}$ is the electric vector field, and $\boldsymbol{e}(=-\nabla T)$ is temperature gradient field. In the indicial notation, by utilizing a notation introduced for a thermoelectric material [60]:

$$J_{Ji} = P_{JiMn}Q_{Mn}, \tag{20}$$

where

$$J_{Ji} = \begin{cases} J_i^E, & J = 1 \\ J_i^S, & J = 2 \end{cases}, \tag{21}$$

$$Q_{Mn} = \begin{cases} E_n, & M = 1 \\ e_n, & M = 2 \end{cases}, \tag{22}$$

$$P_{JiMn} = \begin{cases} \left(\boldsymbol{\sigma}_e\right)_{in}, & J = 1; M = 1 \\ \left(\boldsymbol{\sigma}_e\cdot\boldsymbol{\alpha}\right)_{in}, & J = 1; M = 2 \\ \left(\boldsymbol{\alpha}\cdot\boldsymbol{\sigma}_e\right)_{in}, & J = 2; M = 1 \\ \gamma_{in}/T, & J = 2; M = 2 \end{cases}. \tag{23}$$

In order to find effective properties for the piezoelectric and thermoelectric phenomena using mean-field strategy, the Eshelby tensors for each problem can be found utilizing similar form, considering the mathematical analogy. By representing the steady-state equations as matrix equation $\langle\boldsymbol{p}\rangle = \langle\boldsymbol{X}\rangle\langle\boldsymbol{q}\rangle$ in Mandel notation [61], the effective properties of tensor field $\boldsymbol{X}$ of the composite can be determined using $\langle\boldsymbol{X}_{\text{eff}}\rangle = \left(c_0\langle\boldsymbol{X}_0\rangle + c_1\langle\boldsymbol{X}_1\rangle\langle\boldsymbol{T}\rangle\right)\left(c_0\langle\boldsymbol{I}\rangle + c_1\langle\boldsymbol{T}\rangle\right)^{-1}$ where $\langle\boldsymbol{T}\rangle = \left[\langle\boldsymbol{I}\rangle + \langle\boldsymbol{S}\rangle\langle\boldsymbol{X}_0\rangle^{-1}\left(\langle\boldsymbol{X}_1\rangle - \langle\boldsymbol{X}_0\rangle\right)\right]^{-1}$. Here, $\langle\boldsymbol{p}\rangle$ and $\langle\boldsymbol{q}\rangle$ are $N\times 1$ matrix while $\langle\boldsymbol{X}\rangle$, $\langle\boldsymbol{T}\rangle$, $\langle\boldsymbol{I}\rangle$, and $\langle\boldsymbol{S}\rangle$ are $N\times N$ matrix. The value of N varies depending on the problem: $N = 6$ for elasticity (comprising 6 independent components of the strain tensor), $N = 3$ for conductivity/dielectric (with a 3-dimensional vector field), $N = 9$ for piezoelectricity (6 from the strain tensor and 3 from the electric field), and $N = 6$ for thermoelectricity (3 from the electric field and 3 from the temperature gradient field). The comparisons with FEM predictions for these four properties, depicted as a function of volume fraction, are illustrated in Fig. 4.

When interfacial imperfections are present, similar mathematical analysis can be employed to predict the effective properties. The spring compliance in elasticity is analogous to the Kapitza resistance in thermal conduction, interfacial electric resistance for dielectric response, etc. Hence, for the interfacial imperfection analogous to the interface spring model in elasticity (e.g., Kapitza resistance for thermal conduction), the modified Eshelby tensor can be written as $\boldsymbol{S}^M = \left[\boldsymbol{I} + \frac{\gamma_s}{R}(\boldsymbol{I}-\boldsymbol{S}) : \boldsymbol{X}_0\right]^{-1} : \left[\boldsymbol{S} + \frac{\gamma_s}{R}(\boldsymbol{I}-\boldsymbol{S}) : \boldsymbol{X}_0\right]$, the modified concentration tensor as $\boldsymbol{T}^M = \left[\boldsymbol{I} + \boldsymbol{S} : \boldsymbol{X}_0^{-1} : \left(\boldsymbol{X}_1 - \boldsymbol{X}_0\right) + \frac{\gamma_s}{R}(\boldsymbol{I}-\boldsymbol{S}) : \boldsymbol{X}_1\right]^{-1}$, and the effective physical property tensor as $\boldsymbol{X}_{\text{eff}} = \left(c_0\boldsymbol{X}_0 + c_1\boldsymbol{X}_1 : \boldsymbol{T}^M\right) : \left(c_0\boldsymbol{I} + c_1\boldsymbol{T}^M + c_1\frac{\gamma_s}{R}\boldsymbol{X}_1 : \boldsymbol{T}^M\right)^{-1}$ [46]. The detailed discussion can be found in the literature for conductivity equation [63], piezoelectric equation [57], and thermoelectric equation [59].

Combining Data-Driven Methods

The mean-field homogenization theory relies on a set of mathematical assumptions, and its predictions tend to deviate when these assumptions are not satisfied. These assumptions include: (i) treating reinforcements as ellipsoids, (ii) assuming an infinitely large domain, and (iii) assuming minimal interactions among reinforcements, meaning a low volume fraction. To put it simply, if the reinforcements don't have ellipsoidal shapes, or if the specimen size is relatively small compared to the size of the reinforcements (as is often the case with composite fibers), or if the volume fraction of reinforcements is high, the theory's predictions may not match accurate calculations obtained through numerical simulation or experiment. In addition, in the presence of interfacial imperfection, even ellipsoidal reinforcements or non-equal normal and tangential compliance would result in the deviation when the imperfections are treated with the interface spring model. Furthermore, when predicting the nonlinear stress-strain response under complex and cyclic loading, systematic errors can occur due to numerical calculations or approximations involved in linearization.

To summarize, homogenization allows researchers to quickly estimate the effective properties of composites, albeit with some approximations. In contrast, accurate FEM calculations or experiments provide precise predictions but require more time and cost. In essence, when predicting the properties of composites with varying compositions and constituent materials, the former approach can generate a large but less accurate dataset (low-fidelity), while the latter produces a smaller but more accurate dataset (high-fidelity). By leveraging these two datasets with differing

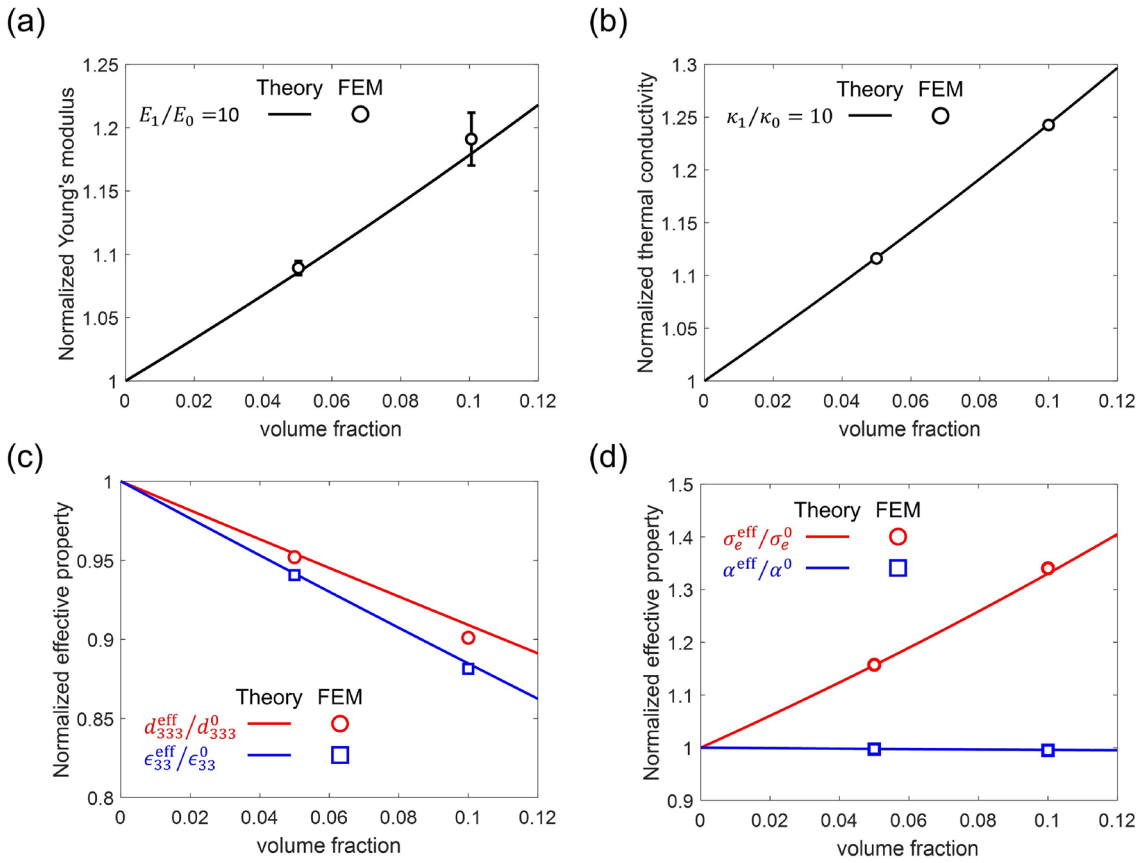

Fig. 4 Effective properties of particulate-reinforced composites plotted against inhomogeneity volume fraction: **a** Normalized Young's modulus, **b** normalized thermal conductivity, **c** normalized piezoelectric constant and dielectric permittivity, and **d** normalized electric conductivity and Seeback coefficient. All effective properties are normalized with respect to corresponding matrix properties. Material properties for piezoelectricity [62] and thermoelectricity [60] are obtained from literature sources. This figure is adopted from Ref. [46] under Creative Commons Attribution Licence (CC BY)

levels of fidelity through suitable data-driven methods, which are typically referred as multi-fidelity methods, it becomes possible to significantly enhance the accuracy and efficiency of composite analyses. For more discussions on data-driven materials modeling including but not limited to multi-fidelity methods, readers can refer to [64].

Considering the limitations in accuracy of homogenization methods and the demanding data requirements of Deep Neural Networks (DNNs), transfer learning techniques can be integrated into composite analysis. Transfer learning is a strategy where a model initially trained for a specific task serves as a foundation for training a second model. This approach is particularly useful when acquiring an ample amount of data is challenging. When dealing with the representative volume element of a composite featuring reinforcements with a high aspect ratio in the nonlinear regime, extensive computational resources are needed for FEM simulations utilizing detailed microstructures. It also is a daunting task to acquire large enough dataset from experiments for DNN. Consequently, obtaining the necessary volume of data for machine learning becomes problematic. Hence, by combining the homogenization theory with transfer learning, one can efficiently and reliably predict the effective behavior of the elasto-plastic composite. Initially, a substantial dataset is generated at a low computational cost using the homogenization theory for the primary DNN training. Subsequently, the pre-trained DNN is fine-tuned using relatively small FEM data obtained through transfer learning. Figure 5 illustrates the transfer learning schematic (Fig. 5a) and showcases the results of stress-strain curve predictions obtained through transfer learning for monotonic (Fig. 5b), and cyclic loading cases (Fig. 5c).

Conclusion

In this paper, a comprehensive exploration of determining effective physical properties utilizing micromechanics-based homogenization theory is presented. To start,

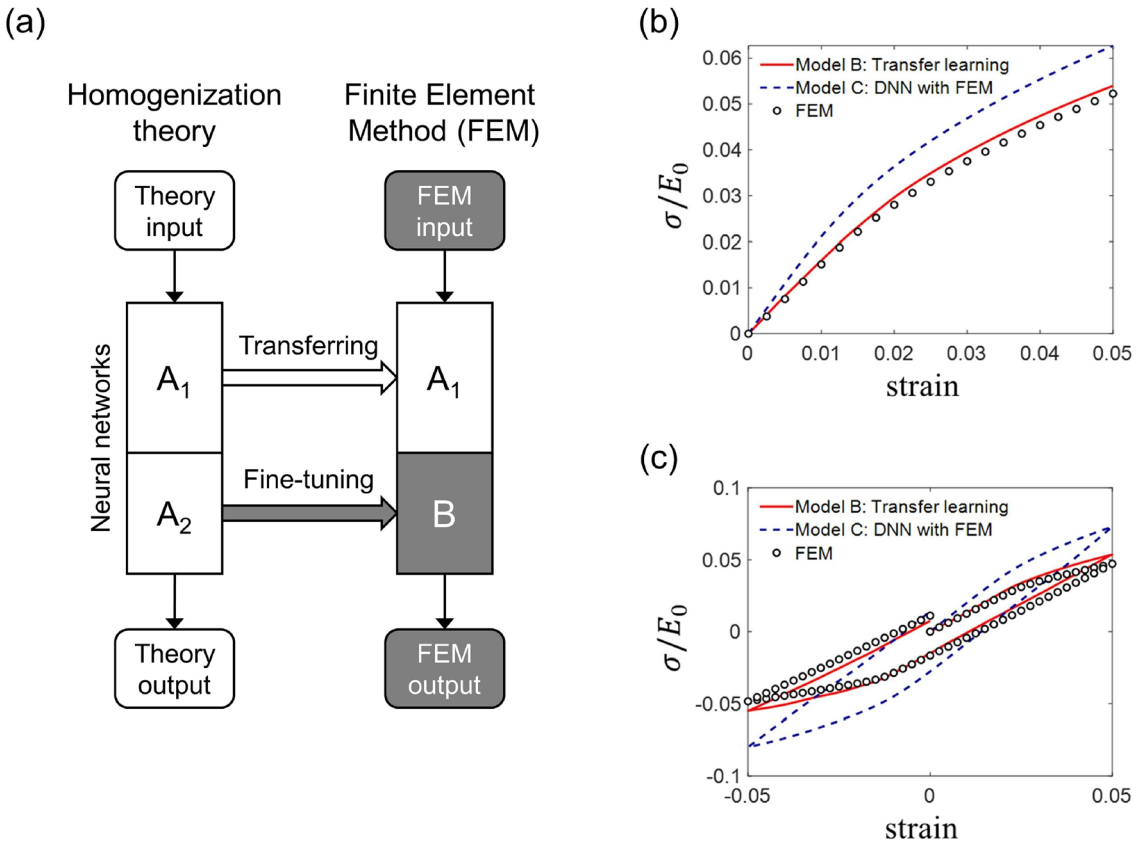

Fig. 5 **a** Schematics of transfer learning technique based on neural networks utilizing homogenization theory data as low-fidelity and FEM numerical simulation data as high-fidelity. Stress-strain curve prediction of neural network with (Model B) and without (Model C) transfer learning: for monotonic (**b**) and cyclic (**c**) loading cases. The data-driven model predictions are compared with FEM results. Reproduction with permission from Ref. [65] Copyright (2022) Elsevier

we use elasticity as a specific case study and introduce the concept of the Eshelby tensor. We delve into the connection between a single-inclusion problem and a single inhomogeneity problem, showcasing its utility in mean-field homogenization for predicting composite properties. Next, we expand the application of our approach to predict nonlinear stress-strain curves beyond the elastic limit, particularly under complex and cyclic loading conditions. We also delve into the impact of interfacial imperfections on the Eshelby tensor, stress concentration tensor, and effective stiffness tensor. Furthermore, we illustrate that mean-field homogenization equations for different physical phenomena can be expressed as equations involving matrices of varying dimensions. Lastly, we discuss how the accuracy of predictions from homogenization theory can be enhanced by incorporating a small but precise dataset from numerical analysis or experimental results using data-driven methods.

The issues related to extension and advancement of homogenization theory can be categorized into five key problems: (i) nonlinear responses under complex and cyclic loading, (ii) imperfections at the matrix-filler interface, (iii) various physical phenomena, (iv) high volume fractions of reinforcements, and (v) localized failure. While substantial research has been conducted on issues (i) to (iv) with promising outcomes as discussed in this article, tackling (v) localized failure remains a significant challenge. To make homogenization theory more practically useful, it is imperative to accurately predict the criteria for localized failure.

Presently, commercial software like Digimat incorporates homogenization theory as a constitutive equation for conducting large-scale structural calculations. However, the failure criteria offered by such software are often limited due to constraints inherent in the mean-field strategy or due to limitations in analytic failure criteria, which restrict their broader applicability. In its original formulation, the mean-field homogenization method lacks the capability to account for stress or strain localization within the microstructure, making it challenging to accurately assess failure criteria arising from highly localized regions. Moreover, handling such localized phenomena can be problematic even with general direct simulation methods that incorporate

continuum damage mechanics, due to potential issues related to the loss of ellipticity in the governing partial differential equation. This loss of ellipticity can lead to the loss of solution uniqueness. To overcome these challenges, higher-order continuum formulations have been employed. In the context of mean-field homogenization, gradient-enhanced damage models [66–68], and integral-type non-local models [69] have been combined to simulate composite failure. It is crucial to acknowledge that these methods often entail a substantial computational cost, thereby mitigating the advantage of the low computational cost typically associated with mean-field schemes in comparison to other multi-scale methods. Therefore, the development of a numerically efficient homogenization scheme for addressing localized failure remains a significant challenge.

Lastly, it is noteworthy that active research is ongoing for the development of homogenization schemes tailored specifically for soft elastic composites. These materials have a wide range of applications, including industrial parts like tires, biological materials for biomedical applications, and elastomeric active materials in soft actuator applications. However, formulating a homogenization framework for such materials presents a significant challenge due to their tendency to undergo extreme deformations, resulting in substantial microstructure evolution as well as macroscopic instabilities. More details on mathematical foundations and modeling results can be found in [70] and references therein.

Acknowledgement This work is financially supported by the National Research Foundation of Korea (NRF) grants funded by the Korea government (MSIT) (No. RS-2023-00249021, 2022R1A2B5B02002365).

Funding Open Access funding enabled and organized by KAIST.

Data availability The data utilized in this review paper were sourced from published literature and publicly available databases. All original sources are referenced within the manuscript. No new data were generated for this review.

Declarations

Conflict of interest The authors declare that they have no known competing financial interests that are directly or indirectly related to the work submitted for publication.

References

1. N.P. Suh, *Axiomatic design and fabrication of composite structures: applications in robots, machine tools, and automobiles* (Oxford University Press, Oxford, 2005), p.1
2. H. Gao, Application of fracture mechanics concepts to hierarchical biomechanics of bone and bone-like materials. Int J Fract **138**, 101–137 (2006)
3. Y. Kim, Y. Kim, T.-I. Lee, T.-S. Kim, S. Ryu, An extended analytic model for the elastic properties of platelet-staggered composites and its application to 3D printed structures. Compos Struct **189**, 27–36 (2018)
4. T. Mura, *Micromechanics of Defects in Solids* (Kluwer Academic Publishers, Dordrecht, The Netherlands, 1987)
5. Y. Benveniste, A new approach to the application of Mori-Tanaka's theory in composite materials. Mech Mater **6**(2), 147–157 (1987)
6. R. Hill, A self-consistent mechanics of composite materials. J Mech Phys Solids **13**(4), 213–222 (1965)
7. P.P. Castañeda, E. Tiberio, A second-order homogenization method in finite elasticity and applications to black-filled elastomers. J Mech Phys Solids **48**(6–7), 1389–1411 (2000)
8. M.I. Idiart, K. Danas, P.P. Castañeda, Second-order theory for nonlinear composites and application to isotropic constituents. Comptes Rendus Mecan **334**(10), 575–581 (2006)
9. I. Doghri, M.I. El Ghezal, L. Adam, Finite strain mean-field homogenization of composite materials with hyperelastic-plastic constituents. Int J Plast **81**, 40–62 (2016)
10. L. Wu, L. Noels, L. Adam, I. Doghri, A combined incremental-secant mean-field homogenization scheme with per-phase residual strains for elasto-plastic composites. Int J Plast **51**, 80–102 (2013)
11. P.P. Castañeda, The effective mechanical properties of nonlinear isotropic composites. J Mech Phys Solids **39**(1), 45–71 (1991)
12. N. Lahellec, P. Suquet, On the effective behavior of nonlinear inelastic composites: I. Incremental variational principles. J Mech Phys Solids **55**(9), 1932–1963 (2007)
13. N. Lahellec, P. Suquet, On the effective behavior of nonlinear inelastic composites: II: A second-order procedure. J Mech Phys Solids **55**(9), 1964–1992 (2007)
14. S. Nemat-Nasser, Averaging theorems in finite deformation plasticity. Mech Mater **31**(8), 493–523 (1999)
15. L. Brassart, L. Stainier, I. Doghri, L. Delannay, A variational formulation for the incremental homogenization of elasto-plastic composites. J Mech Phys Solids **59**(12), 2455–2475 (2011)
16. J.D. Eshelby, The determination of the elastic field of an ellipsoidal inclusion, and related problems. Proc R Soc London Series A Math Phys Sci **241**(1226), 376–396 (1957)
17. J.D. Eshelby, The elastic field outside an ellipsoidal inclusion. Proc R Soc London Series A Math Phys Sci **252**(1271), 561–569 (1959)
18. S. Lee, S. Ryu, Theoretical study of the effective modulus of a composite considering the orientation distribution of the fillers and the interfacial damage. Eur J Mech-A/Solids **72**, 79–87 (2018)
19. C. Friebel, I. Doghri, V. Legat, General mean-field homogenization schemes for viscoelastic composites containing multiple phases of coated inclusions. Int J Solids Struct **43**(9), 2513–2541 (2006)

20. Z. Hashin, Viscoelastic behavior of heterogeneous media. J Appl Mech **32**, 630 (1965)
21. Z. Hashin, Complex moduli of viscoelastic composites—I. General theory and application to particulate composites. Int J Solids Struct **6**(5), 539–552 (1970)
22. R. Christensen, Viscoelastic properties of heterogeneous media. J Mech Phys Solids **17**(1), 23–41 (1969)
23. O. Pierard, I. Doghri, An enhanced affine formulation and the corresponding numerical algorithms for the mean-field homogenization of elasto-viscoplastic composites. Int J Plast **22**(1), 131–157 (2006)
24. O. Pierard, J.L. Lorca, J. Segurado, I. Doghri, Micromechanics of particle-reinforced elasto-viscoplastic composites: finite element simulations versus affine homogenization. Int J Plast **23**(6), 1041–1060 (2007)
25. R. Masson, A. Zaoui, Self-consistent estimates for the rate-dependentelastoplastic behaviour of polycrystalline materials. J Mech Phys Solids **47**(7), 1543–1568 (1999)
26. O. Pierard, *Micromechanics of inclusion-reinforced composites in elasto-plasticity and elasto-viscoplasticity: modeling and computation* (Universit catholique de Louvain, Belgium, 2006), p.1
27. P.P. Castaneda, Second-order homogenization estimates for nonlinear composites incorporating field fluctuations: I—theory. J Mech Phys Solids **50**(4), 737–757 (2002)
28. L. Brassart, L. Stainier, I. Doghri, L. Delannay, Homogenization of elasto-(visco) plastic composites based on an incremental variational principle. Int J Plast **36**, 86–112 (2012)
29. G. Weng, The overall elastoplastic stress-strain relations of dual-phase metals. J Mech Phys Solids **38**(3), 419–441 (1990)
30. G. Hu, Composite plasticity based on matrix average second order stress moment. Int J Solids Struct **34**(8), 1007–1015 (1997)
31. I. Doghri, L. Adam, N. Bilger, Mean-field homogenization of elasto-viscoplastic composites based on a general incrementally affine linearization method. Int J Plast **26**(2), 219–238 (2010)
32. B. Miled, I. Doghri, L. Brassart, L. Delannay, Micromechanical modeling of coupled viscoelastic–viscoplastic composites based on an incrementally affine formulation. Int J Solids Struct **50**(10), 1755–1769 (2013)
33. P.P. Castañeda, Exact second-order estimates for the effective mechanical properties of nonlinear composite materials. J Mech Phys Solids **44**(6), 827–862 (1996)
34. O. Pierard, I. Doghri, Study of various estimates of the macroscopic tangent operator in the incremental homogenization of elastoplastic composites. Int J Multiscale Comput Eng **4**(4), 521 (2006)
35. J. Chaboche, P. Kanouté, A. Roos, On the capabilities of mean-field approaches for the description of plasticity in metal matrix composites. Int J Plast **21**(7), 1409–1434 (2005)
36. Y. Kim, J. Jung, S. Lee, I. Doghri, S. Ryu, Adaptive affine homogenization method for Visco-hyperelastic composites with imperfect interface. Appl Math Model **107**, 72–84 (2022)
37. J. Jung, Y. Kim, S. Lee, I. Doghri, S. Ryu, Improved incrementally affine homogenization method for viscoelastic-viscoplastic composites based on an adaptive scheme. Composit Struct **297**, 115982 (2022)
38. Z. Sekkate, A. Aboutajeddine, A. Seddouki, Elastoplastic mean-field homogenization: recent advances review. Mech Adv Mater Struct **29**(3), 449–474 (2022)
39. I. Doghri, L. Brassart, L. Adam, J.-S. Gérard, A second-moment incremental formulation for the mean-field homogenization of elasto-plastic composites. Int J Plast **27**(3), 352–371 (2011)
40. J. Qu, The effect of slightly weakened interfaces on the overall elastic properties of composite materials. Mech Mater **14**(4), 269–281 (1993)
41. S. Lee, J. Lee, S. Ryu, Modified Eshelby tensor for an anisotropic matrix with interfacial damage. Math Mech Solids **24**(6), 1749–1762 (2019)
42. S. Lee, Y. Kim, J. Lee, S. Ryu, Applicability of the interface spring model for micromechanical analyses with interfacial imperfections to predict the modified exterior Eshelby tensor and effective modulus. Math Mech Solids **24**(9), 2944–2960 (2019)
43. Y. Qiu, G. Weng, Elastic moduli of thickly coated particle and fiber-reinforced composites. J Appl Mech **58**, 388 (1991)
44. H. Duan, J. Wang, Z. Huang, Z. Luo, Stress concentration tensors of inhomogeneities with interface effects. Mech Mater **37**(7), 723–736 (2005)
45. M. Dunn, H. Ledbetter, Elastic moduli of composites reinforced by multiphase particles. J Appl Mech **62**, 1023 (1995)
46. S. Ryu, S. Lee, J. Jung, J. Lee, Y. Kim, Micromechanics-based homogenization of the effective physical properties of composites with an anisotropic matrix and interfacial imperfections. Front Mater **6**, 21 (2019)
47. Z. Zhong, S.A. Meguid, On the elastic field of a spherical inhomogeneity with an imperfectly bonded interface. J Elast **46**(2), 91–113 (1997)
48. J. Qu, M. Cherkaoui, *Fundamentals of micromechanics of solids* (Wiley Online Library, UK, 2006), p.1
49. S. Lee, J. Jung, S. Ryu, Applicability of interface spring and interphase models in micromechanics for predicting effective stiffness of polymer-matrix nanocomposite. Extreme Mech Lett **49**, 101489 (2021)
50. S. Yang, M. Cho, Scale bridging method to characterize mechanical properties of nanoparticle/polymer nanocomposites. Appl Phys Lett (2008). https://doi.org/10.1063/12965486
51. G.W. Milton, *The Theory of Composites* (Cambridge University Press, Cambridge, UK, 2002)
52. G.K. Batchelor, Transport properties of two-phase materials with random structure. Ann Rev Fluid Mech **6**(1), 227–255 (1974)
53. E.J. Rothwell, M.J. Cloud, *Electromagnetics* (CRC Press, US, 2018), p.1
54. R.B. Bird, W.E. Stewart, E.N. Lightfoot, *Transport Phenomena*, 2nd edn. (Wiley, New York, 2002), p.1
55. J. Welty, G.L. Rorrer, D.G. Foster, *Fundamentals of momentum, heat, and mass transfer* (Wiley, New York, 2020), p.1
56. S. Whitaker, Flow in porous media I: A theoretical derivation of Darcy's law. Trans Porous Media **1**, 3–25 (1986)
57. S. Lee, J. Jung, S. Ryu, Micromechanics-based prediction of the effective properties of piezoelectric composite having interfacial imperfections. Composit Struct **240**, 112076 (2020)
58. D.M. Barnett, J. Lothe, Dislocations and line charges in anisotropic piezoelectric insulators. Phys Status Solidi (b) **67**(1), 105–111 (1975)
59. J. Jung, W. Demeke, S. Lee, J. Chung, B. Ryu, S. Ryu, Micromechanics-based theoretical prediction for thermoelectric properties of anisotropic composites and porous media. Int J Thermal Sci **165**, 106918 (2021)
60. J. Jung, S. Lee, B. Ryu, S. Ryu, Investigation of effective thermoelectric properties of composite with interfacial resistance using micromechanics-based homogenisation. Int J Heat Mass Trans **144**, 118620 (2019)
61. P. Helnwein, Some remarks on the compressed matrix representation of symmetric second-order and fourth-order tensors. Comput Method Appl Mech Eng **190**(22–23), 2753–2770 (2001)
62. G.M. Odegard, Constitutive modeling of piezoelectric polymer composites. Acta Mater **52**(18), 5315–5330 (2004)
63. S. Lee, J. Lee, B. Ryu, S. Ryu, A micromechanics-based analytical solution for the effective thermal conductivity of composites with orthotropic matrices and interfacial thermal resistance. Sci Rep **8**(1), 1–11 (2018)

64. J. Lee, D. Park, M. Lee, H. Lee, K. Park, I. Lee, S. Ryu, Machine learning-based inverse design methods considering data characteristics and design space size in materials design and manufacturing: a review. Mater. Horiz. **10**, 5436–5456 (2023). https://doi.org/10.1039/D3MH00039G
65. J. Jung, Y. Kim, J. Park, S. Ryu, Transfer learning for enhancing the homogenization-theory-based prediction of elasto-plastic response of particle/short fiber-reinforced composites. Composit Struct **285**, 115210 (2022)
66. L. Wu, L. Noels, L. Adam, I. Doghri, A multiscale mean-field homogenization method for fiber-reinforced composites with gradient-enhanced damage models. Comput Method Appl Mech Eng **233**, 164–179 (2012)
67. L. Wu, L. Noels, L. Adam, I. Doghri, An implicit-gradient-enhanced incremental-secant mean-field homogenization scheme for elasto-plastic composites with damage. Int J Solids Struct **50**(24), 3843–3860 (2013)
68. L. Wu, F. Sket, J.M. Molina-Aldareguia, A. Makradi, L. Adam, I. Doghri, L. Noels, A study of composite laminates failure using an anisotropic gradient-enhanced damage mean-field homogenization model. Composit Struct **126**, 246–264 (2015)
69. P. Lenz, R. Mahnken, Non-local integral-type damage combined to mean-field homogenization methods for composites and its parallel implementation. Composit Struct **314**, 116911 (2023)
70. P.P. Castañeda, Soft elastic composites: Microstructure evolution, instabilities and relaxed response by domain formation. Eur J Mech-A/Solids **100**, 105033 (2023)